Anomalous refractive properties of a two-dimensional photonic band-gap prism

J. Bravo-Abad, T. Ochiai,* and J. Sánchez-Dehesa†

Departamento de Física Teórica de la Materia Condensada, Facultad de Ciencias (C-V), Universidad Autónoma de Madrid, Madrid 28049, Spain

An analysis of the optical response of a triangular-shaped photonic band-gap prism is presented. Numerical simulations have been performed in the framework of multiple-scattering theory, which is applied considering spot illumination to avoid diffraction effects. First of all, refractive properties in the frequency range below the first TM band gap are analyzed and compared with the available experimental data. It validates the approach employed and supports the predictions obtained in the frequency range above the gap. At these high frequencies we found an unusual superprism effect characterized by an angle sensitivity and a frequency sensitivity of the intensity of outgoing beams. We report several representative examples that could be used in device applications. The results are interpreted in terms of the corresponding semi-infinite photonic crystal, through the analysis of the coupling between external radiation and bulk eigenmodes, using the two-dimensional-layer-Korringa-Kohn-Rostoker method. The procedure presented here constitutes a simple but functional alternative to the methods used until now with the same purpose.

I. INTRODUCTION

Since the seminal works of Yablonovitch[1] and John,[2] photonic crystals (PC's) have generated a great interest, both in fundamental and applied physics. These materials could have an important role in the development of the photonic information technology. This is especially true in the case of two-dimensional (2D) PC's due to their easy fabrication by standard lithographic techniques. On the other hand, recent advances in growing techniques are also allowing the fabrication of planar devices based on three-dimensional (3D) systems.[3]

The study of optical properties of PC using numerical tools[4–7] is an essential procedure in order to further increase the understanding of physical properties of PC's. The potential applications of PC's has motivated the development of efficient theoretical methods that allow us to obtain realistic comparisons between theory and experiments. One of the most versatile methods is the multiple-scattering method (MSM). Its formalism is based on the expansion of the 2D (3D) radiation field in cylindrical (spherical) harmonics centered at each scattering object, and it has been successfully applied in the analysis of interaction of radiation with dielectric and metallic finite 2D and 3D structures.[8–17]

Several authors have analyzed the optical response of structures based on 2D PC's.[18–22] Recently, 2D PC's with nonparallel boundaries have been investigated both numerically, by using the finite-difference-time-domain (FDTD) method,[23] and experimentally.[24] However, a complete theoretical analysis including the study of the coupling between incident radiation and bulk eigenmodes is still lacking.

The goal of this work is to present a comprehensive analysis of the optical properties of a photonic band-gap prism by using the multiple-scattering formalism and other numerical techniques. The prism, which has a triangular shape, consists of a hexagonal array of nonoverlapping dielectric cylinders of infinite height. The analysis is made in the low-frequency region (below the first TM band gap),

where a comparison with available experimental data[25] is presented, and also in the frequency domain above the first TM band gap, where anomalous refractive properties are predicted. The results of the MSM simulations are interpreted in terms of the corresponding semi-infinite PC. Moreover, in order to get a physical insight of the optical response in this structure, we also have made quantitative predictions of the coupling strength between the incident light and the bulk eigenmodes that can be excited; i.e., the eigenmodes that satisfy the kinetic matching conditions at the air/PC interface. A complete theoretical analysis by means of a combination of plane wave expansion (PWE) and 2D-layer-Korringa-Kohn-Rostoker (2D-LKKR) method allows us to get accurate predictions which could be confirmed experimentally. The good agreement found between theoretical results and available experiments supports the different approaches employed.

In our studies, we have found an unusual superprism phenomenon, in which the intensity of outgoing beams shows a dependence on both the frequency and incident angle of the external beam. This differs from the superprism effect reported until now,[26] where large dependence is found only in outgoing beams directions. Also, it must be emphasized that this work provides simple but working guidelines to design functionalities of superprism structures based on a 2D photonic band gap systems. On the other hand, this work also shows that the MSM is competitive with the time-demanding FDTD method in order to simulate actual 2D structures.

The paper is organized as follows. In Sec. II, we describe briefly the basis of the MSM employed to study the optical response of the prism. The results of numerical simulations and the discussion in terms of the semi-infinite model is presented in Sec. III. Finally, in Sec. IV, we summarize the work.

II. NUMERICAL METHOD

Here, the MSM is applied to study a finite lattice of dielectric cylinders of (of dielectric constant ϵ_r) infinite height

embedded in a background of different dielectric constant ϵ_b. For a complete description of the numerical algorithm employed, see, for example, the paper by Ochiai and Sánchez-Dehesa,[15] and references therein. In brief, the numerical simulations are based on the solution of the following self-consistent equation:[8–17]

$$\tilde{\psi}_\alpha^{ind} = t_\alpha \left(\tilde{\psi}_\alpha^{ext} + \sum_{\beta \neq \alpha} G_{\alpha\beta} \tilde{\psi}_\beta^{ind} \right), \tag{1}$$

where the field $\psi = E_z (H_z)$ for TM (TE) polarization. $\tilde{\psi}_\alpha^{ind}$ in Eq. (1) is a column vector that contains the components of the multipole expansion of the radiation field induced by the cylinder α centered at $\mathbf{r}_\alpha$, $\tilde{\psi}_\alpha^{ext}$ represents the external wave, t_α is the t matrix, and $G_{\alpha\beta}$ is the propagator from cylinder β to α.

Most of the previous simulations using the 2D MSM employed an incident wave having a plane wave front as external source . However, in the case under study here, a structure with nonparallel boundaries, it is necessary to use spot illumination in order to avoid diffraction effects. Moreover, spot illumination is essential to make comparisons with available experiments,[25] which use collimated beams in the microwave regime. So far, to the best of our knowledge, there have been two different procedures to simulate a collimated beam: (1) the first one defines a finite aperture in front of the sample.[10,11] (2) the second one simulates the spot illumination by using a Gaussian beam.[20,27,28] We have demonstrated that, for our system, a Gaussian beam is more appropriate because it reproduces the measurements fairly well.

The incident Gaussian beam of frequency ω, focusing at $\mathbf{r}_0$, can be expressed as the following very directional solution of the homogeneous Helmholtz equation:[29]

$$\psi^{ext}(\mathbf{r}) = \int_{-k_0}^{k_0} dk_y e^{-Dk_y^2} e^{i\mathbf{k}(\mathbf{r} - \mathbf{r}_0)}, \tag{2}$$

where $\mathbf{r}$ is the position vector, which in polar coordinates becomes $\mathbf{r} = (r, \theta)$. $\mathbf{k}$ is the wave vector of a plane wave in the beam, $\mathbf{k} = (k_x, k_y)$, where $k_x = \sqrt{k_0^2 - k_y^2}$, and $k_0 = \omega\sqrt{\epsilon_b}/c$. Parameter D determines the width of the beam.

Therefore, the ℓth component of the external field is given as

$$\psi_{\alpha,\ell}^{ext} = i^\ell k_0 \int_{-\pi/2}^{\pi/2} d\theta \cos\theta e^{g_1(\theta) + ig_2(\theta)}, \tag{3}$$

where

$$g_1(\theta) = -Dk_0^2 \sin^2\theta,$$

$$g_2(\theta) = k_0\{r_\alpha \cos(\theta + \theta_{inc} - \theta_\alpha) - r_0 \cos(\theta + \theta_{inc} - \theta_0)\} - \ell\theta, \tag{4}$$

and $(r_\alpha, \theta_\alpha)$ and (r_0, θ_0) are the polar coordinates of the αth cylinder and the focusing point, respectively.

We are interested in the far-field response of the structure. It can be easily found that in the far-field regime,[30]
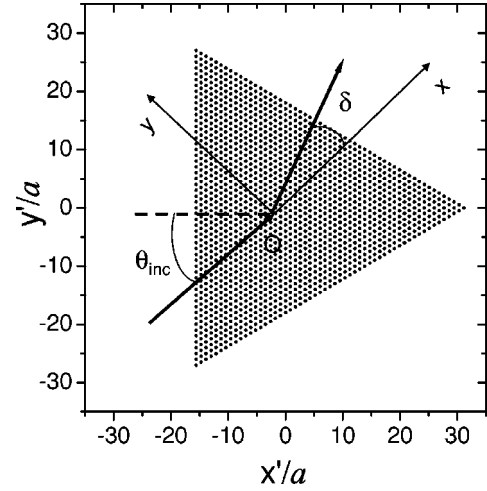

FIG. 1. Schematic view of the triangular prism under study and parameter definitions. The reference system used in the calculation is also plotted.

$$\psi^{ext}(\mathbf{r}) \rightarrow \begin{cases} a_0(\theta) e^{ik_0 r}/\sqrt{r} & \text{if } -\dfrac{\pi}{2} \leq \theta \leq \dfrac{\pi}{2} \\[2mm] a_0(\theta - \pi) e^{-ik_0 r}/\sqrt{r} & \text{otherwise,} \end{cases} \tag{5}$$

where $a_0(\theta) = \sqrt{2\pi k_0} e^{-i(\pi/4)} e^{-Dk_0^2 \sin^2\theta} \cos\theta$.

The magnitude of interest in this problem is the intensity at infinity (I_s). It is defined by the Poynting vector flux per unit angle calculated at far field;

$$I_s(\theta) = \begin{cases} |a_0(\theta) + f_s(\theta)|^2 & \text{if } -\dfrac{\pi}{2} \leq \theta \leq \dfrac{\pi}{2} \\[2mm] |f_s(\theta)|^2 - |a_0(\theta)|^2 & \text{otherwise,} \end{cases} \tag{6}$$

where $f_s(\theta)$ is the scattering amplitude, which is obtained from Eq. (1) as a linear combination of $\psi_{\alpha,\ell}^{ind}$ (Ref. 15).

III. RESULTS AND DISCUSSION

The optical response to TM-polarized light of a 2D photonic band gap prism based on a hexagonal array of 1540 alumina rods ($\epsilon_r = 8.9$) in air ($\epsilon_b = 1.0$) is studied. In order to compare with the experiments performed by Lin *et al.*,[25] the radius of cylinders is set to $r = 0.188a$, where a is the lattice parameter. The external shape of the prism is triangular: the three boundaries of the prism are composed of 55 cylinders each, and they are parallel to the ΓK direction. A scheme of the structure and the definitions of incident angle θ_{inc} and deviation angle δ are shown in Fig. 1. The system of reference used along the calculations is also plotted.

The photonic band structure for TM-polarized modes of the corresponding infinite lattice, which has been calculated by means of a plane-wave expansion,[31] is plotted in Fig. 2, where the frequencies are given in reduced units. A factor of $2\pi c/a$ (c is the light velocity in air) must be used to obtain the absolute values. So, in the rest of the paper, the frequency is given in reduced units. Results in Fig. 2 indicate that a complete band gap exists between $\omega_L = 0.325$ and $\omega_U = 0.497$.
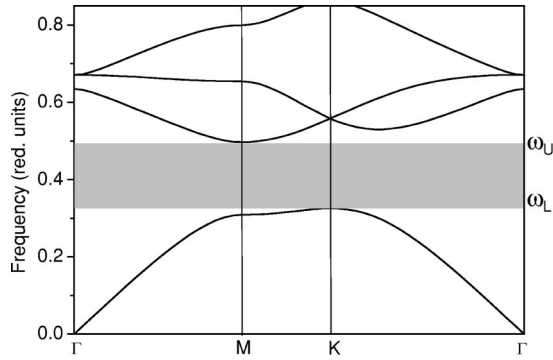
FIG. 2. Photonic band structure for TM-polarized modes corresponding to a hexagonal lattice of dielectric cylinders ($\epsilon_r = 8.9$) in air ($\epsilon_b = 1.0$). The cylinder radius is $r = 0.188a$, where a is the lattice constant. The shaded region defines the complete band gap.

First of all, frequencies inside the band gap were examined in order to check whether the bulk properties of the hexagonal lattice were already achieved. Let us consider a frequency slightly greater than ω_L, for instance, 0.33. The electric field pattern computed for the case of normal incidence ($\theta_{inc} = 0°$), $D = 20a^2$, and $\mathbf{r}_0 = 0$ is visualized in Fig. 3. It can be seen that no light propagates inside the prism and, therefore, this frequency is inside the photonic band gap, which is in agreement with the photonic band structure shown in Fig. 2.

In what follows, we report the optical response in two different regimes, below and above the first photonic TM band gap. We obtained converged results by considering $\ell = 1$ as the maximum angular momentum for frequencies below the band gap, and $\ell = 2$ for the frequencies considered above the band gap.

A. Behavior at frequencies below the first TM band gap

In the very low-frequency region, the equifrequential curves are circles and, therefore, it is possible to define an effective refraction index independent of incident angle.[18]
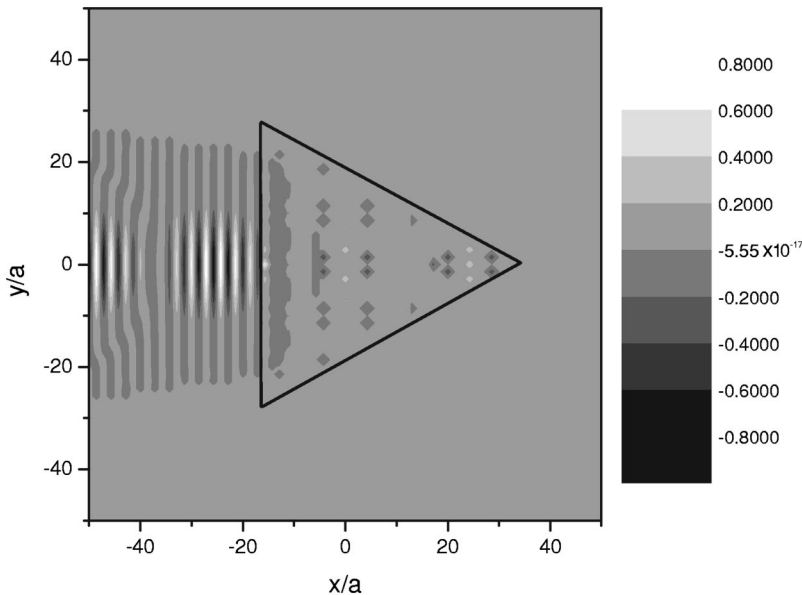
It can be stated that, by using the MSM and for frequencies below the first TM band gap, it is possible to accurately find the deviation angle of the beam transmitted across the prism only by assuming certain $\mathbf{r}_0 \neq 0$ and D values large enough.[32]

In addition, the asymmetry observed in the transmitted peaks can be explained by the Fresnel factor because of the fact that the incident beam is represented by superposition of plane waves with different incident angles and different weights [Eq. (2)].

A procedure to get the effective refractive index (n_{eff}) from the MSM is to fit the numerical results (θ_{inc}, δ) to the expression obtained applying Snell's law in the case of non-parallel boundaries structure with a homogeneous n_{eff}:

$$\delta = \theta_{inc} + \sin^{-1}[(\sin\alpha)(n_{eff}^2 - \sin^2\theta_{inc})^{1/2}$$
$$- \sin\theta_{inc}\cos\alpha] - \alpha, \qquad (7)$$

where α is the prism angle, which is 60° for the triangular prism under analysis. Figure 4 shows the dependence of δ on θ_{inc} for several angles at $\omega = 0.26$ (black dots). The solid line corresponds to a fit of MSM data to Eq. (7). From this fit, $n_{eff} = 1.54$ is obtained. Experimentally, Lin et al.[25] reported $n_{eff} \approx 1.57$ (dashed line in Fig. 4). Therefore, our simulations based on the MSM confirms that at this low frequency ($\omega = 0.26$), the refractive index does not depend on θ_{inc} and, moreover, its value fairly agrees with experimental data (about 2% of relative error).

The previous considerations allow us to analyze theoretically the optical response for all frequencies below the first band gap. Unfortunately, we found that the contribution of the transmitted beam for frequencies near the band edge are not clearly observed in the calculations (its transmission is almost zero). In other words, the scattered intensity is mainly determined by the shape of the prism. The result is summarized in Fig. 5(a), where n_{eff} obtained from the MSM simulations (black dots) are compared with experimental data (white circles) and with a simplified model (solid line) that
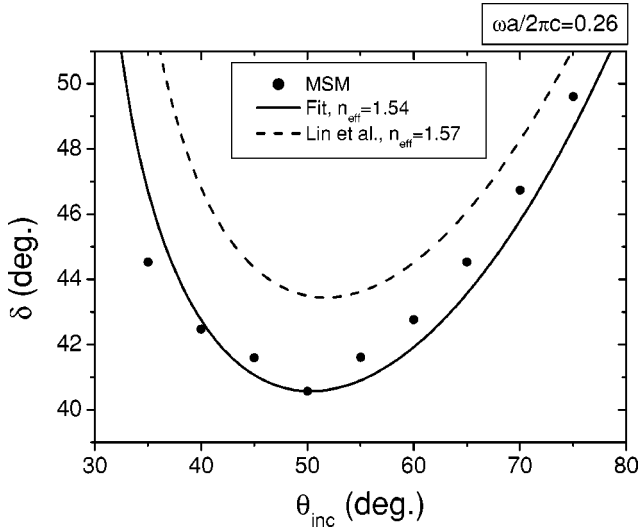

FIG. 3. Electric field pattern, $E_z(x,y)$ generated by a Gaussian beam, with the parameters $D = 20a^2$, $r_0 = 0$, and $\omega = 0.33$, impinging on the prism.

FIG. 4. Dependence of deviation angle δ on incident angle θ_{inc} for $\omega = 0.26$ (solid points). Solid line is obtained by fitting Eq. (7). $n_{eff} = 1.54$ is obtained from this fit. Dashed line corresponds to experimental results.

considers light propagation across single air/PC interfaces (see Appendix A). The previous approach predicts a sharp decrease of n_{eff} near the band edge, which, unfortunately, is confirmed neither by the MSM nor by the experimental setup due to their intrinsic limitations. Figure 5(b) shows the behavior of n_{eff} as a function of θ_{inc}. It can be observed that, as it is expected, n_{eff} does not depend on θ_{inc} at low frequencies, but near the band edge, the critical frequency at which n_{eff} starts to decrease depends on θ_{inc}. This phenomenon is a result of the shape of the equifrequencial curves near the band edges. This prediction should stimulate more accurate experimental works looking for its demonstration.

Finally, let us remark that small discrepancies observed between experimental and numerical results can be mainly attributed to the fact that the actual beam used experimentally is not well enough simulated by the 2D numerical beam introduced in the simulations by the MSM. In other words, the spot size and collimation of a 2D Gaussian beam cannot be controlled to reproduce accurately the properties of the actual beam. This is the main drawback of the simulations based on the MSM, which produces fictitious diffraction effects. Fortunately, for higher frequencies, these effects disappear, and is possible to characterize interesting phenomena as it is reported in what follows.

B. Behavior above the first TM band gap

In order to study the optical response in frequencies above the first complete TM band gap, we have started by analyzing the case of infinite structures and have chosen the ranges of frequency and incident angle, at which anomalous phenomena are expected when light crosses an air/PC interface. Equifrequencial curves between 0.509 and 0.627 are plotted in Fig. 6(a). Notice that near the curves associated to frequency 0.537 [thick lines in Fig. 6(a)], the equifrequencial curves consist of two separated regions: a hexagonal-shaped
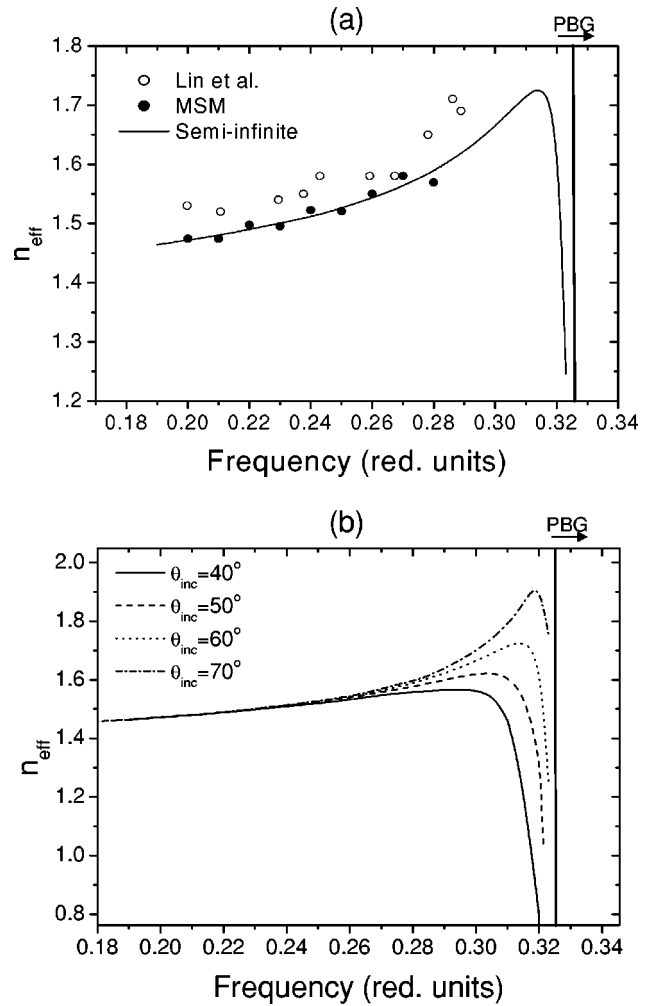

FIG. 5. (a) Behavior of the effective refractive index n_{eff} as a function of frequency. Hollow points correspond to experimental data, solid points to MSM simulations, and solid line to the simplified model (see text). (b) Dependence of n_{eff} as a function of the frequency for different incident angles θ_{inc} computed by the simplified model.

region (centered at Γ point) and a triangular-shaped region (centered at K point). Therefore, it is expected that such anisotropic equifrequencial regions lead to anomalous response of a finite structure based on the same lattice periodicity.

The procedure described in Appendix A allows us to compute the propagating angle θ_{pro} inside the PC as a function of the incident angle for a beam crossing the air/PC interface at $\omega = 0.537$. The result of this calculation, which is depicted in Fig. 6(b), shows that above a critical angle θ_c, the incident beam splits into two. They correspond to the curves of frequency 0.537 which have group velocity with positive y component. The great dependence of θ_{pro} on θ_{inc} of these solutions from 20° to 25° and from 25° to 40° is associated to the rounded corners of the hexagonal- and triangular-shaped regions, respectively.

A comprehensive analysis of the scattering properties in the frequency range between 0.5 and 0.6 and for incident angles between 20° and 40° has been performed by using the MSM. This analysis has allowed us to select the most interesting phenomena.
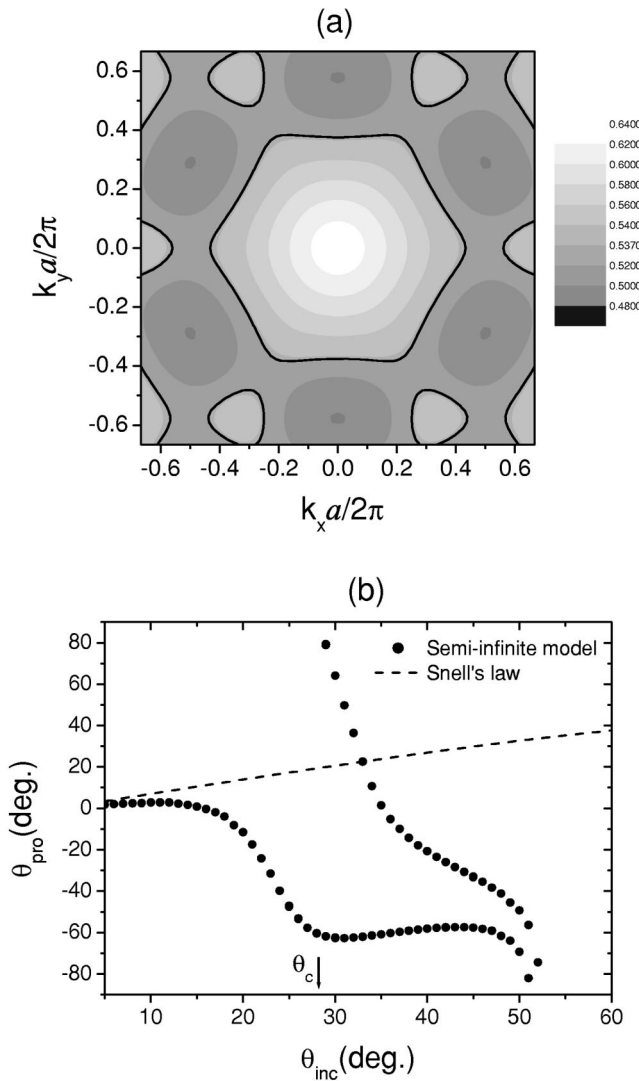
(a)

(b)

FIG. 6. (a) Equifrequencial curves for the photonic TM bands in Fig. 2. Curves for frequencies between 0.509 and 0.627 are represented. Solid line corresponds to $\omega = 0.537$. (b) Dependence of the propagation angle on the incident angle considering $\omega = 0.537$. Dashed line is the result of Snell's law calculated by considering a uniform medium with a spatially averaged refractive index $n_{ave} = 1.419$.

Figure 7(a) shows the intensity map as a function of δ and θ_{inc} computed with $\omega = 0.537$. The parameters of the Gaussian beam employed in both simulations[33] are $D = 30a^2$ and $y_0 = 10a$. As can be seen from this figure, we do not obtain a great dependence of δ as a function of θ_{inc} as could be expected in the usual definition of superprism effect. Instead, we obtain an angular sensitivity of transmitted beam intensities. In order to prove clearly this anomalous effect, Fig. 7(b) shows the comparison between intensity spectrum corresponding to the incident angle with largest transmission ($\theta_{inc} = 22.8°$), and the spectra corresponding to incident angles that differ in $3.2°$. As it is shown in this figure, a small change in θ_{inc} implies a dramatic fall in the transmittance.
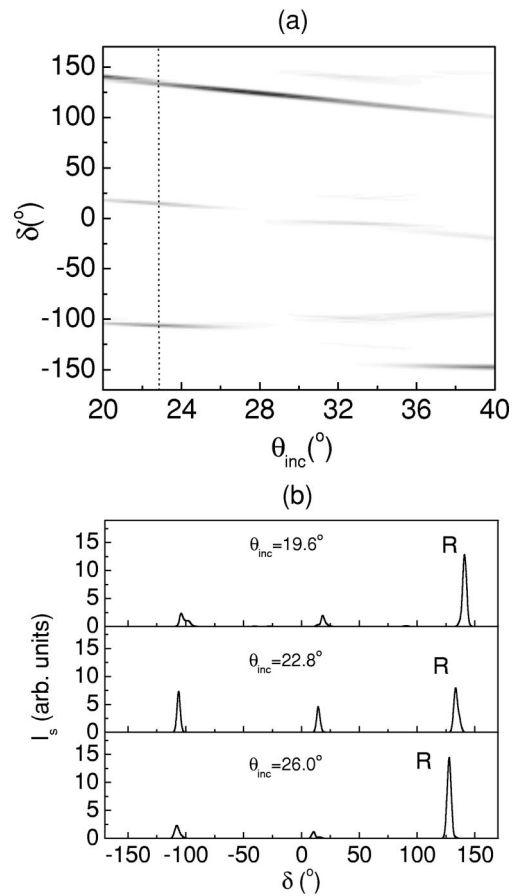

(a)

(b)

FIG. 7. (a) Intensity map as a function of the deviation angle δ and the incident angle θ_{inc} computed with $\omega = 0.537$. White corresponds to zero values and black to the maximum intensity. Dashed line defines the incident angle in which a maximum of the transmittance is found. (b) Comparison between the intensity spectra corresponding to the same frequency ($\omega = 0.537$) and three different angles. R labels the peak corresponding to the reflected intensity. Notice the angular sensitivity of intensity features.

In addition, it is interesting to know the dependence of I_s on ω and δ for $\theta_{inc} = 22.8°$. The result of this calculation is shown in Fig. 8(a). This second transmitted beam only appears in a very narrow range of frequencies; i.e., from 0.533 up to 0.582 approximately. In order to show quantitatively this effect, Figure 8(b) shows a sharp change in the intensity features of the spectra for very small variations (about 0.7%) of frequency. Again we obtain a refractive effect characterized by the large frequency sensitivity in the intensity of the outgoing beams.

The phenomena mentioned previously suggest the above configuration as a sensitive beam splitter, both in angle and frequency regimes.

A similar analysis to the one described previously was carried out for another frequency of interest, $\omega = 0.539$. The corresponding intensity map, with θ_{inc} and δ as variables, is plotted in Fig. 9(a). From this figure, we have selected the angle $\theta_{inc} = 40°$ as the most interesting case. Figure 9(b) shows its corresponding intensity spectrum compared with the spectra associated to two angles differing in $5.2°$. As can
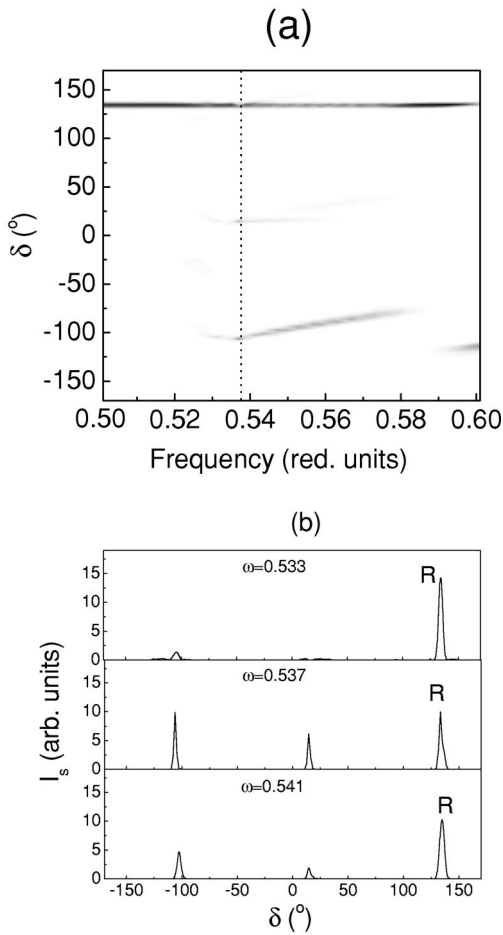
FIG. 8. (a) Intensity map as a function of the deviation angle δ and the frequency ω computed with $\theta_{inc}=22.8°$. White corresponds to zero values and black to the maximum intensity. Dashed line shows the frequency in which a maximum of the transmittance is found. (b) Comparison between the intensity spectra corresponding to the same incident angle ($\theta_{inc}=22.8°$) and three different frequencies. R labels the peak corresponding to the reflected intensity. Notice the frequency sensitivity of intensity features.

be seen from this figure, the main transmitted beam found at $\theta_{inc}=40°$ disappears completely for $\theta_{inc}=34.8°$, while it is almost the same for $\theta_{inc}=45.2°$.

Also we have made a frequency analysis by fixing θ_{inc} at $40°$. The results are summarized in Fig. 10(a), where it is seen that the main transmitted beam only exists in two separated frequency regions. Particularly, Fig. 10(b) shows the behavior in the region centered at $\omega=0.539$. Notice that a change in frequency of about 4% implies a sharp decrease in the transmission of the incident radiation through the prism. Therefore, this configuration could be suitable for the design of a PC filter for a short range of frequencies. A similar conclusion could be obtained for frequencies above 0.58, where the prism is almost transparent and the transmitted beam undergoes a small deviation angle ($\delta \approx -20°$).

Physical insight of the mechanism originating the phenomena observed in Figs. 7–10, can be obtained from the 2D-LKKR method.[35,36] In fact, we have implemented a 2D version of the procedure proposed by two of us in a previous
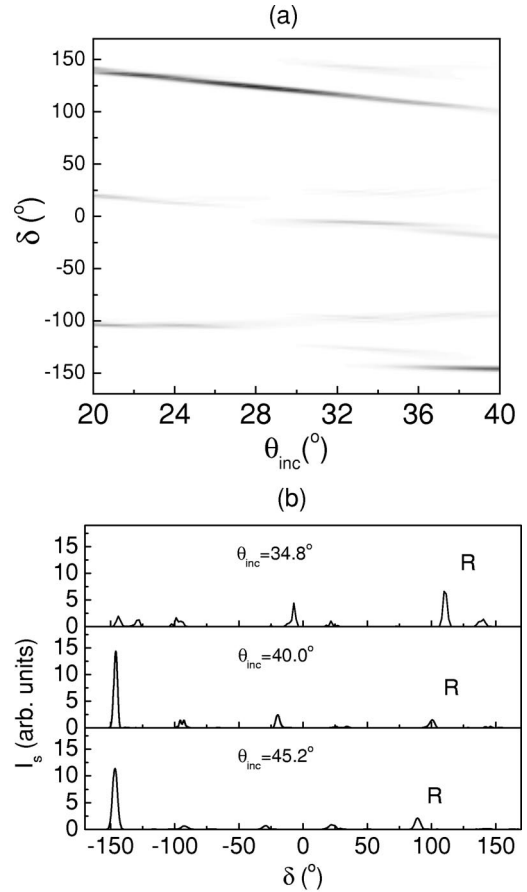

FIG. 9. (a) Intensity map as a function of the deviation angle δ and the incident angle θ_{inc} computed with $\omega=0.539$. White corresponds to zero values and black to the maximum intensity. (b) Comparison between the intensity spectra corresponding to the same frequency ($\omega=0.539$) and three different angles. R labels the peak corresponding to the reflected intensity. Notice the angular sensitivity of intensity features between the top and the center spectra.

work[34] (see Appendix B). In this way, it is possible to obtain the branching ratio (BR) of the different bulk eigenstates of the PC that can couple to the incident light.

In the following, we will refer to the configurations defined by $(\omega, \theta_{inc})=(0.537, 22.8°)$ and $(\omega, \theta_{inc})=(0.539, 40.0°)$ as case 1 and case 2, respectively.

In case 1 (see Fig. 11), simulations using the MSM predict that in addition to the reflected beam R at the front air/PC interface ($133.27°$), two transmitted beams appear: one of them at $-105.82°$ (T_1) and another at $14.42°$(T_2). In this case, if we apply the kinetic matching conditions to the frontal air/PC interface, we obtain that only one eigenstate, with group velocity inward the PC, couples to the incident light. The perpendicular component $k_\perp$ of this eigenstate wave vector ($\mathbf{k}_{pro}$) to the boundary is -0.3592 (in units of $2\pi/a$) [see inset in Fig. 11(b)]. A similar analysis can be performed at boundary 2 in Fig. 11(a). Since boundaries 1 and 2 are not parallel, it is necessary to make a $60°$ rotation of $\mathbf{k}_{pro}$ before applying the matching conditions. As a result of this analysis, we conclude that an output beam should appear at $\delta= -105.48°$, in good agreement with the MSM-based simula-
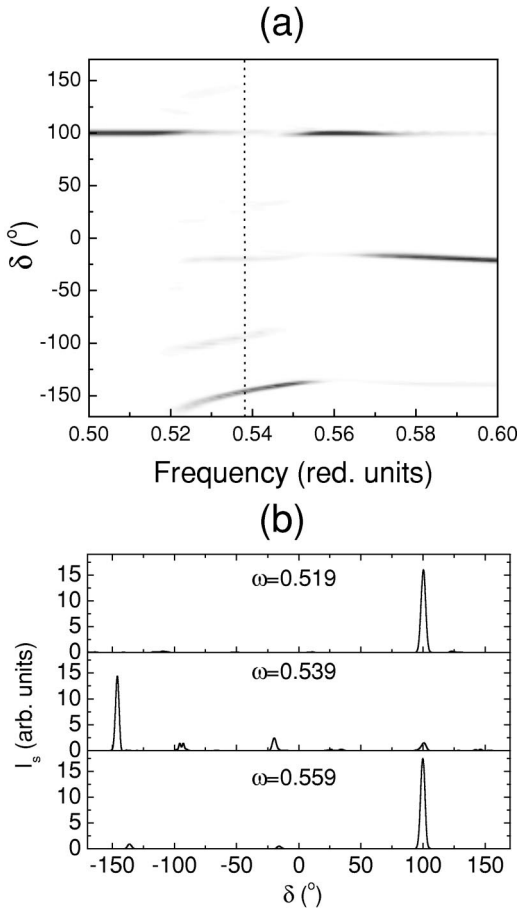
FIG. 10. (a) Intensity map as a function of the deviation angle δ and the frequency ω computed with $\theta_{inc} = 40.0°$. White corresponds to zero values and black to the maximum intensity. Dashed line defines the frequency in which a maximum of the transmittance is found. (b) Comparison between the intensity spectra corresponding to the same incident angle ($\theta_{inc} = 40.0°$) and three different frequencies. Notice the great frequency sensitivity of intensity features.

tions. Also we have to consider the reflection in boundary 2 and the following refraction in boundary 3. For this path, the predicted deviation angle is 14.4°, and we expect small intensity for this peak since it comes from considering two refractions and one reflection. On the other hand, from the 2D-LKKR, it is possible to obtain the reflectance of the corresponding semi-infinite PC at this incident angle. The reflectance is about 0.544. This result is supported by the MSM, where the intensity of the peak associated with the reflected beam (R in Fig. 11) is related to the intensity of the incident beam by that factor.

The field pattern and transmission spectrum obtained from the MSM-based simulations for case 2 ($\omega = 0.539$ and $\theta_{inc} = 40°$) are plotted in Figs. 12(a) and 12(b), respectively. A very small reflected peak (R) appears at 101.16°. The main transmitted beam (T_1) with negative refraction index appears at $-146.16°$, while two secondary transmitted beams are seen at -93.24 (T_2) and $-19.98°$ (T_3). This result can be understood in terms similar to the preceding
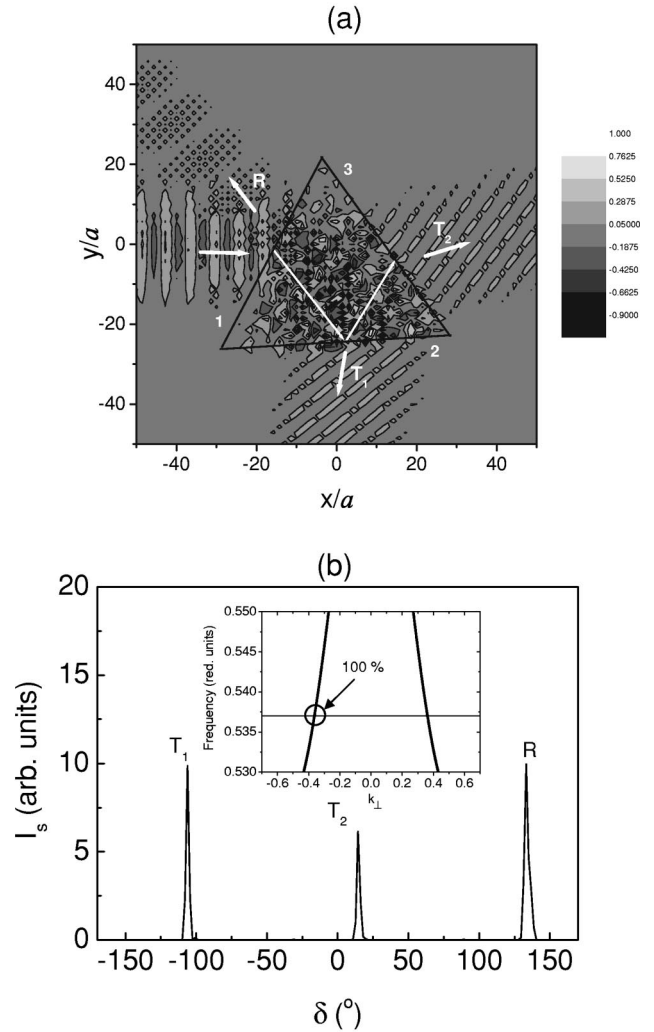

FIG. 11. (a) Electric field pattern and (b) transmission spectra generated from a Gaussian beam with $\omega = 0.537$ and $\theta_{inc} = 22.8°$. White arrows indicate the direction of the group velocity computed by the semi-infinite model (see Appendix A). The solutions to $k_\perp$ and the BR value are shown in the inset.

case, in other words, by analyzing the light transmission through single interfaces. Now we have two eigenstates satisfying the kinetic matching conditions at the frontal interface; their $k_\perp$ values inside the PC, in units of $2\pi/a$, are 0.5095 and -0.1237 [see inset in Fig. 12(b)], and the corresponding BRs are 0.923 and 0.077, respectively. The reflectance of the corresponding semi-infinite PC is about 0.085. This value of the reflectance is in accordance with the small intensity peak of the reflected beam in comparison with the main transmitted beam. The matching conditions applied to boundary 2 in Fig. 12(b) concludes that the first outgoing beam should appear at $\delta = -145.75°$, in good agreement with the MSM results. If we also take into account the beam with negative $k_\perp$, we obtain that a second outgoing beam appears at $\delta = -93.0°$ (also in agreement with Fig. 12). The great difference between the two intensities of these two refracted beams could be estimated using the BR values. Moreover, for the path corresponding to the light reflected at
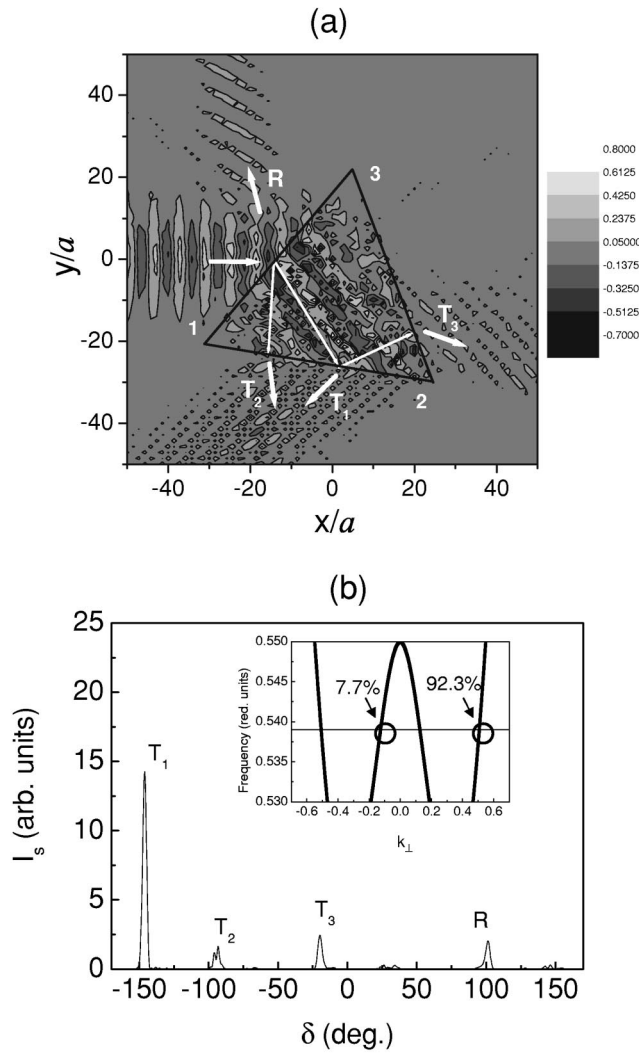
FIG. 12. (a) Electric field pattern and (b) transmission spectra generated from a Gaussian beam with $\omega=0.539$ and $\theta_{inc}=40°$. White arrows indicate the direction of the group velocity computed by the semi-infinite model (see Appendix A). The solutions to $k_\perp$ and the corresponding BR values are shown in the inset.

the boundary 2 and refracted at boundary 3, the predicted deviation angle is $-20.0°$ and we also expect a secondary refracted beam, since the dominant eigenstate in boundary 2 is the refraction.

Table I summarizes the results regarding the directionality of the scattered light. It demonstrates that the deviation angle

TABLE I. Comparison of the deviation angles (in degrees) of beams transmitted across the prism. The results under the columns "Model" are obtained by the procedure described in Appendix A.

| | $\omega=0.537$, $\theta_{inc}=22.8°$ | | $\omega=0.539$, $\theta_{inc}=40°$ | |
	MSM	Model	MSM	Model
T_1 beam	-105.82	-105.48	-146.16	-145.75
T_2 beam	14.42	14.40	-93.28	-93.00
T_3 beam			-19.98	-20.00

of the transmitted light through nonparallel boundaries can be predicted by a simplified model based on the light transmission across semi-infinite air/PC interfaces. Its results agree fairly well with the complete simulation of the finite system performed by MSM-based simulations. In other words, the combination of the Hellmann-Feynmann theorem in the plane-wave expansion, together with the 2D-LKKR method is enough to analyze the optical response of these kind of structures in the high-frequency region.

IV. SUMMARY

In this work, we have analyzed the optical response of a triangular prism made of a hexagonal array of dielectric cylinders in air. The approach employed, based on the multiple-scattering formalism, has been supported by the available experimental data existing at frequencies below the first TM band gap. Also, we have predicted anomalous superprism phenomena above the first TM band gap. A comprehensive analysis in this high-frequency region has been performed by combining the PWE method and the 2D-LKKR method. We have demonstrated that, if the prism is large enough (diffraction effects are negligible), a procedure based in the analysis of the corresponding semi-infinite system agrees very well with the simulation of the complete finite system by the MSM. We have described two cases with possible device application. The results presented in this work support the applied procedure as an efficient numerical tool in the understanding of the optical response in 2D-PC structures with nonparallel boundaries. We hope that this work motivates further experiments that confirm its predictions. Finally, the procedure here employed has been also extended to study analogously 3D prisms composed of PC's having a strong anisotropy in its photonic dispersion relation, and the results will be presented in a forthcoming publication.

APPENDIX A: LIGHT TRANSMISSION ACROSS A SINGLE AIR/PC INTERFACE

Let us assume a semi-infinite 2D PC defined in region $y>0$, and air in the another semiplane. In order to know which eigenstates of the PC can be excited by an external light, it is important to project the bulk photonic band structure on the surface Brillouin zone (SBZ). A typical projected band diagram is shown in Fig. 13. This figure represents the band structure projected on the ΓK boundary surface, which is the common boundary surface of the triangular prism under study. In Fig. 13 the shaded regions define the allowed bulk eigenstates and the thick black line defines the light
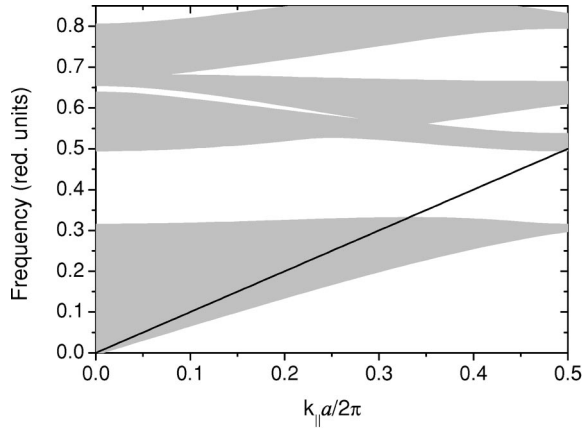
FIG. 13. Projection of the photonic band structure shown in Fig. 2 on the surface Brillouin zone of the ΓK surface. The shaded regions defines the bulk eigenmodes. The frequencies of the external radiation field are defined above the light line (black line), $\omega \geq ck_{\parallel}$.

line. This line defines the critical frequency, above which external plane waves are allowed to exist. The white regions represent pseudogaps in the dispersion relation. Therefore, external beams having frequencies in a pseudogap cannot enter into the PC, as it is shown in Fig. 3.

Another criterion of coupling arises from the group velocity of the bulk eigenmodes. Only the bulk eigenstates with positive v_y can couple with the incident light. Those eigenstates with $v_y < 0$ should be physically neglected.

In summary, the kinetic matching condition between the bulk eigenmodes and the incident light are the following: (1) The frequency and the reduced wave vector in the SBZ are conserved, (2) the bulk eigenmodes are above the light line, and (3) v_y is positive. Once these conditions are satisfied, the incident angles θ_{inc} and the propagating angles θ_{pro}, which are given by

$$k = \frac{\omega}{c}(\sin\theta_{inc}, \cos\theta_{inc}), \tag{A1}$$

$$v = |v|(\sin\theta_{pro}, \cos\theta_{pro}) \tag{A2}$$

can be related through an effective refraction index n_{eff} defined as

$$\sin(\theta_{inc}) = n_{eff}\sin\left(\arctan\left(\frac{v_x}{v_y}\right)\right), \tag{A3}$$

where (v_x, v_y) are the components of the group velocity, which are computed directly from the dispersion relations by using the Hellmann-Feynman theorem.

APPENDIX B: BRANCHING RATIO

Figure 2 shows that at high frequencies, several eigenmodes can be kinetically matched to the external light.

Hence, it is necessary to know quantitatively what is the coupling strength between the incident light and the bulk eigenstates of the 2D PC. Here, the 2D-layer-KKR method is used for that purpose in a similar manner as was employed in its 3D counterpart in the analysis of the superprism effect in opals.[34]

We have considered a slab large enough for the deepest region in the slab to be regarded as a superposition of the actual bulk eigenstates α; i.e., the field at this central region is assumed not be affected by the finite size of the slab. In the 2D-LKKR method, three different regions can be clearly separated: (1) Left region, defined by the scattering matrix Q_L; (2) center or the deepest region; (3) and right region, whose scattering matrix is Q_R. If we consider that a plane wave impinges the slab from the left, the following relationships are satisfied:[34,35]

$$\begin{pmatrix} \mathbf{E}_d^+ \\ \mathbf{E}_{ref} \end{pmatrix} = \begin{pmatrix} Q_{++}^L & Q_{+-}^L \\ Q_{-+}^L & Q_{--}^L \end{pmatrix} \begin{pmatrix} \mathbf{E}_{inc} \\ \mathbf{E}_d^- \end{pmatrix}, \tag{B1}$$

$$\begin{pmatrix} \mathbf{E}_{tr}^+ \\ \mathbf{E}_d^- \end{pmatrix} = \begin{pmatrix} Q_{++}^R & Q_{+-}^R \\ Q_{-+}^R & Q_{--}^R \end{pmatrix} \begin{pmatrix} \mathbf{E}_d^+ \\ 0 \end{pmatrix}, \tag{B2}$$

where $\mathbf{E}_{inc}$, $\mathbf{E}_{ref}$, $\mathbf{E}_{tr}$ are column vectors which contain the Fourier components of the incident, reflected, and transmitted fields, respectively. $\mathbf{E}_d$ corresponds to the field in the inner void region of the slab, "$+$" denotes propagation from left to right and "$-$" from right to left.

From Eqs. (B1) and (B2), it is easy to obtain

$$\mathbf{E}_d^+ = (1 - Q_{+-}^L Q_{-+}^R)^{-1} Q_{++}^L \mathbf{E}_{inc}, \tag{B3}$$

$$\mathbf{E}_d^- = Q_{-+}^R (1 - Q_{+-}^L Q_{-+}^R)^{-1} Q_{++}^L \mathbf{E}_{inc}. \tag{B4}$$

Let us consider the αth left eigenstate $(\mathbf{V}_{\alpha,L}^{\pm})$ of the transfer matrix which relates the Fourier components of the electric field between two consecutive voids in a infinite PC. It is possible to define the projection of the eigenstate in the deepest void of the slab in the true αth eigenstate through the coefficients c_α defined by

$$c_\alpha = (\mathbf{V}_{\alpha,L}^+)^* \mathbf{E}_d^+ + (\mathbf{V}_{\alpha,L}^-)^* \mathbf{E}_d^-. \tag{B5}$$

These coefficients allows to define the BR (given by script R_α) corresponding to the bulk eigenstates,

$$\mathcal{R}_\alpha = \frac{|c_\alpha|^2}{\sum_{\alpha'} |c_{\alpha'}|^2}, \tag{B6}$$

where the summation is over all the bulk states satisfying the kinetic matching condition. So, $\mathcal{R}_\alpha$ gives an estimation of the coupling of the external light with the αth bulk eigenstates in the 2D PC, and it is normalized to the total coupling of eigenstates available for light transmission.

*Current address: Center for Frontier Science, Chiba University, Chiba 263-8522, Japan.

†Electronic address: jose.sanchezdehesa@uam.es

[1] E. Yablonovitch, Phys. Rev. Lett. **58**, 2059 (1987).

[2] S. John, Phys. Rev. Lett. **58**, 2486 (1987).

[3] S.M. Yang, H. Míguez and G.A. Ozin, Adv. Funct. Mater. **12**, 425 (2002).

[4] J.D. Joannopoulos, R.D. Meade, and J.N. Winn, *Photonic Crystals* (Princeton University Press, Princeton, 1995).

[5] K. Sakoda, *Optical Properties of Photonic Crystals* (Springer-Verlag, Berlin, 2001).

[6] *Photonic Crystals and Light Localization,* edited by C. M. Soukoulis (Kluwer, Dordrecht, 2001).

[7] K. Busch, C. R. Phys. **3**, 53 (2002).

[8] D. Felbacq, G. Tayeb, and D. Maystre, J. Opt. Soc. Am. A **11**, 2526 (1994).

[9] G. Tayeb and D. Maystre, J. Opt. Soc. Am. A **14**, 3323 (1997).

[10] L.M. Li and Z.Q. Zhang, Phys. Rev. B **58**, 9587 (1998).

[11] L.M. Li, Z.Q. Zhang and X. Zhang, Phys. Rev. B **58**, 15 589 (1998).

[12] Y. Chow, L.M. Li, Z.Q. Zhang, and C.T. Chan, Phys. Rev. B **60**, 8050 (1999).

[13] J. Yonekura, M. Ikeda, and T. Baba, IEEE J. Lightwave Technol. **17**, 1500 (1999).

[14] S. Nojima, Appl. Phys. Lett. **79**, 1959 (2001).

[15] T. Ochiai and J. Sánchez-Dehesa, Phys. Rev. B **65**, 245111 (2002).

[16] E. Moreno, D. Erni, and C. Hafner, Phys. Rev. B **65**, 155120 (2002).

[17] F.J. Garcia de Abajo, Phys. Rev. B **60**, 6086 (1999); Phys. Rev. Lett. **82**, 2776 (1999).

[18] M. Notomi, Phys. Rev. B **62**, 10 696 (2000).

[19] P. Halevi, A.A. Krokhin, and J. Arriaga, Phys. Rev. Lett. **82**, 719 (1999).

[20] S. Enoch, G. Tayeb, and D. Maystre, Opt. Commun. **161**, 171 (1999).

[21] C. Luo, S.G. Johnson, J.D. Joannopoulos, and J.B. Pendry, Phys. Rev. B **65**, 201104(R) (2002).

[22] K.B. Chung and S.W. Hong, Appl. Phys. Lett. **81**, 1549 (2002).

[23] T. Baba and M. Nakamura, IEEE J. Quantum Electron. **38**, 909 (2002).

[24] L. Wu, M. Mazilu, T. Karle, and T. Krauss, IEEE J. Quantum Electron. **38**, 915 (2002).

[25] S.Y. Lin, V.M. Hietala, L. Wang, and E.D. Jones, Opt. Lett. **21**, 1771 (1996).

[26] H. Kosaka, T. Kawashima, A. Tomita, M. Notomi, T. Tamamura, T. Sato, and S. Kawakami, Phys. Rev. B **58**, R10096 (1998).

[27] B. Gralak, S. Enoch, and G. Tayeb, J. Opt. Soc. Am. A **17**, 1012 (2000).

[28] G. Pelosi, A. Cocchi, and A. Monorchio, IEEE Trans. Antennas Propag. **48**, 973 (2000).

[29] M. Nieto-Vesperinas, *Scattering and Diffraction in Physical Optics* (Wiley, New York, 1991).

[30] See, for example, P. Sheng, *Introduction to Wave Scattering, Localization and Mesoscopic Phenomena* (Academic Press, San Diego, 1995).

[31] S.G. Johnson and J.D. Joannopoulos, Opt. Express **8**, 173 (2001).

[32] For $\theta_{inc} \leqslant 55°$, diffraction effects can be avoided by considering $\mathbf{r}_0 = (010)$. Besides, owing to a Gaussian beam tends to a plane wave for D large enough, the deviation angle δ of the main transmitted beam converges to a certain value as D increases. This converged value, obtained at $D = 30a^2$, is the one employed in the following simulations.

[33] In this frequency range, the result is almost independent of these parameters since the beam is very collimated and diffraction effects are negligible.

[34] T. Ochiai and J. Sánchez-Dehesa, Phys. Rev. B **64**, 245113 (2001).

[35] K. Ohtaka, T. Ueta, and K. Amemiya, Phys. Rev. B **57**, 2550 (1998).

[36] A. Moroz, Opt. Lett. **26**, 1119 (2001).